Polyion Complex Vesicles for Photoinduced Intracellular Delivery of Amphiphilic Photosensitizer

Huabing Chen,[○,†,‡] Ling Xiao,[○,§] Yasutaka Anraku,[‡] Peng Mi,[∥] Xueying Liu,[§] Horacio Cabral,[∥] Aki Inoue,[‡] Takahiro Nomoto,[∥] Akihiro Kishimura,*[,‡,⊥] Nobuhiro Nishiyama,*[,#,▽] and Kazunori Kataoka*[,‡,§,∥,#]

[†]Jiangsu Key Laboratory of Translational Research and Therapy for Neuro-Psycho-Diseases, and College of Pharmaceutical Sciences, Soochow University, Suzhou 215123, China

[‡]Department of Materials Engineering, Graduate School of Engineering, The University of Tokyo, 7-3-1 Hongo, Bunkyo-ku, Tokyo 113-8656, Japan

[§]Center for Disease Biology and Integrative Medicine, Graduate School of Medicine, The University of Tokyo, 7-3-1 Hongo, Bunkyo-ku, Tokyo 113-0033, Japan

[∥]Department of Bioengineering, Graduate School of Engineering, The University of Tokyo, 7-3-1 Hongo, Bunkyo-ku, Tokyo, 113-8656, Japan

[⊥]Center for Molecular Systems & Department of Applied Chemistry, Faculty of Engineering, Kyushu University, 744 Moto-oka, Nishi-ku, Fukuoka 819-0395, Japan

[#]Center for NanoBio Integration (CNBI), The University of Tokyo, 7-3-1 Hongo, Bunkyo-ku, Tokyo 113-8656, Japan

[▽]Polymer Chemistry Division, Chemical Resources Laboratory, Tokyo Institute of Technology, 4259 Nagatsuta, Midori-ku, Yokohama 226-8503, Japan

Ⓢ Supporting Information

ABSTRACT: Polymer vesicles formed by a pair of oppositely charged poly(ethylene glycol) (PEG)-based block aniomer and homocatiomer, termed "PICsomes", have tunable size, and are characterized by unique semipermeable property due to the flexible and tunable hydrophilicity of polyion complex (PIC) membranes. The PICsomes can encapsulate a variety of molecules in an inner aqueous phase just by a simple vortex mixing of solution, expecting their utility as nanocontainers of substances with biomedical interests. Here, we report on a new functionality of the PICsomes: photoinduced release of photoactive agents for intracellular drug delivery. A potent photosensitizer, Al(III) phthalocyanine chloride disulfonic acid (AlPcS2a), was efficiently incorporated into the PICsomes (11%(w/w)), and its quick release was induced by photoirradiation possibly due to the photochemical damage of the PIC membranes. The combination of a high-resolution fluorescent confocal microscopy and a lysosome membrane-specific staining method revealed that such photoinduced release of AlPcS2a occurred even in the lysosomes of living cells after endocytic internalization. Simultaneously, the released AlPcS2a photochemically affected the integrity of the lysosomal membranes, leading to the translocation of AlPcS2a and PICsomes themselves to the cytoplasm. Consequently, the AlPcS2a-encapsulated PICsomes (AlPcS2a-PICsomes) exhibited appreciably stronger photo-cytotoxicity compared with free AlPcS2a alone. Thus, the AlPcS2a-PICsomes have promising feasibility for the photodynamic therapy or the photoinduced cytoplasmic delivery of therapeutic molecules.
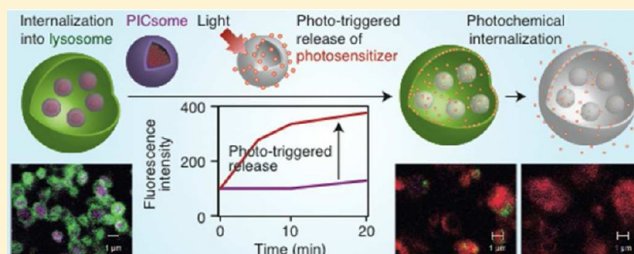
INTRODUCTION

Supramolecular assemblies from block copolymers have been receiving intensive attention in the fields of biomedical applications.[1] We have recently reported polyion complex vesicles (PICsomes),[2] which are self-assembled from a pair of oppositely charged PEG-based block aniomer and homocatiomer. Compared with polymersomes from amphiphilic block copolymers, PICsomes have some unique characteristics. For example, the size of PICsomes can be precisely controlled between 100 and 400 nm, by changing the concentration of the component polymers.[2b] Loading of therapeutics can be achieved by simply vortex mixing in aqueous milieu without using any organic solvents.[2b] Furthermore, the PICsomes membrane can be cross-linked in a controlled manner to tune the stability and the permeability, which leads to a controlled release of payloads in physiological environment.[2b,c] In this study, we wish to report a novel biomedical application of the

PICsomes, adequately exploiting their unique properties as smart nanocontainers with tunable permeability: photoinduced release of cargo molecules (photoactive agents) in intracellular compartment directing to improved photodynamic efficacy.

Photodynamic therapy (PDT) is a powerful approach for selectively destroying cancer cells by highly reactive singlet oxygen or free radical species generated by PSs upon light irradiation at a proper wavelength.[3] Moreover, a certain type of PSs can be used to selectively disrupt endo/lysosomal membranes. This strategy is called photochemical internalization (PCI) and has been successfully employed to release a large variety of endocytosed molecules, such as doxorubicin, bleomycin, peptides, and nucleic acids, into the cytosol of cells.[4] Typical PSs for PCI have amphiphilic nature, such as Al(III) phthalocyanine chloride disulfonic acid (AlPcS2a) and tetraphenylporphine disulfonate (TPPS2a). To improve the efficacy and safety of PDT and PCI, nanoscaled vehicles (nanocontainers) can be applied for the site-specific delivery of these PSs, because they can selectively accumulate in solid tumors due to the enhanced permeability and retention (EPR) effect.[5] However, it is still difficult to satisfy both efficient encapsulation and desirable release rate of amphiphilic PS with conventional nanocontainers approaches.[6] For instance, core–shell polymeric micelles are usually difficult to retain relatively hydrophilic compounds. Liposomes and polymersomes can encapsulate amphiphilic compounds in their inner aqueous phase, but they are difficult to release their contents in a desirable rate.[7] Unlike these conventional nanocontainers, the cross-linked PICsomes achieved efficient encapsulation of AlPcS2a and photoinduced release property inside living cells as described below.

RESULTS AND DISCUSSION

The block aniomer poly(ethylene glycol)$_{45}$-poly(α,β-aspartic acid)$_{75}$ (PEG$_{45}$-(PAsp)$_{75}$) and homocatiomer poly([5-amino-pentyl]-α,β-aspartamide)$_{82}$ (homo-P(Asp-AP)$_{82}$) were synthesized according to the previous reported method.[2a,d] PEG$_{45}$-(PAsp)$_{75}$ and homo-P(Asp-AP)$_{82}$ were mixed, and then free AlPcS2a was further added to the above solution under vortex mixing, followed by the subsequent addition of 1-ethyl-3-(3-dimethylaminopropyl) carbodiimide hydrochloride (EDC) (10 equivalent per −COOH group in PEG-P(Asp)) for cross-linking the membranes of PICsomes. Finally, the cross-linked AlPcS2a-loaded PICsomes (AlPcS2a-PICsomes) were purified by ultrafiltration (Cut-off 100 K MW) at 4 °C (Scheme 1). The average hydrodynamic size of AlPcS2a-PICsomes measured by dynamic light scattering is ~106 nm with a polydispersity index
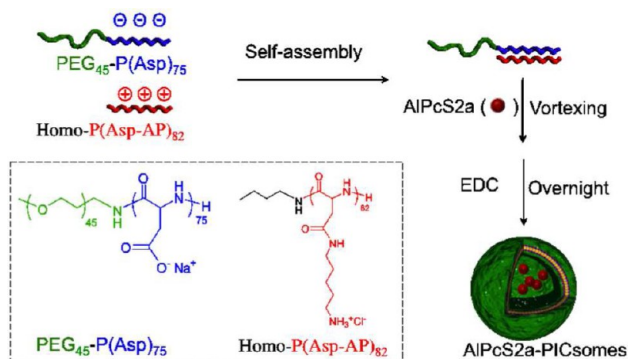
of 0.09 (Figure 1a). The zeta potential (ζ) of blank PICsomes ranged between −3.0 and −5.0 mV. After AlPcS2a loading or
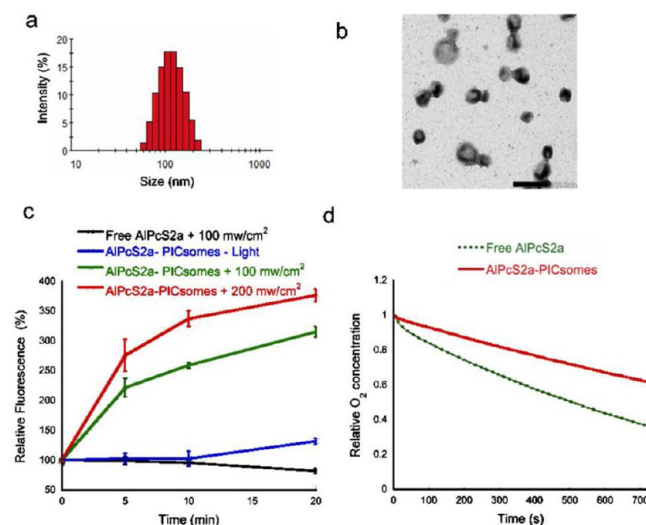

Figure 1. Characterization of AlPcS2a-PICsomes. (a) Size distribution by dynamic light scattering. (b) TEM image of AlPcS2a-PICsomes, the scale bar is 200 nm. (c) Increase in fluorescence intensity of AlPcS2a-PICsomes as a function of irradiation time in the dark, 100 and 200 mW/cm^2. Illumination was accomplished with a NIR 680 nm laser. (d) Comparison of oxygen consumption between AlPcS2a-PICsomes and free AlPcS2a in 10 mM PB (pH 7.4) containing 10% FBS under irradiation.

Cy3 labeling (the cyanine dye Cy3 was covalently attached to the aniomer PEG$_{45}$-(PAsp)$_{75}$), the zeta potentials of AlPcS2a-PICsomes and Cy3 labeled AlPcS2a-PICsomes remained in the same range at both pH 7.4 and pH 5.0 (representing endo/lysosomal pH environment). This can be explained by the PEG shielding of the negative charge of AlPcS2a.[8] It indicates that the loaded therapeutics and the exterior pH had no influence on the zeta potential of the PICsomes, implying that the PICsomes can be applied to incorporate various therapeutic molecules without changing its physical properties. Transmission electron microscope (TEM) imaging showed that AlPcS2a-PICsomes exhibited a uniform vesicular morphology (Figure 1b), consistent with the DLS measurement. Free AlPcS2a was removed from AlPcS2a-PICsomes by ultrafiltration at 4 °C, leading to a drug loading of 11% (w/w), which was preferable to that of other vesicular nanocontainers.

It is worth noting that the AlPcS2a as an amphiphilic PS tends to aggregate in the entrapped state, thereby decreasing its fluorescence intensity and photoactivity due to the self-quenching effect induced by dimerization in 10 mM PB (Figure S1, Supporting Information).[9] Such AlPcS2a aggregation can be disrupted by the treatment with 0.1 M NaOH, obtaining the fluorescence of AlPcS2a in a free form. By comparing the fluorescence intensities of AlPcS2a-PICsomes in 10 mM PB and 0.1 M NaOH, we estimated that ~95% of the core-loaded AlPcS2a presented in aggregation state. Also, based on the recovery of the fluorescence intensities of AlPcS2a-PICsomes, we can estimate the release of AlPcS2a monomer from the PICsomes.

In this study, we found that the recovery of the fluorescence intensities of AlPcS2a-PICsomes was induced by photo-irradiation (Figure 1c). In this experiment, the relative fluorescence intensities of AlPcS2a-PICsomes before irradiation

Scheme 1. Schematic Illustration of AlPcS2a-PICsomes

158

dx.doi.org/10.1021/ja406992w | J. Am. Chem. Soc. 2014, 136, 157−163

(0 min) and after 5, 10, and 20 min of irradiation with NIR 680 nm laser at both 100 and 200 mW/cm^2 were recorded. Upon 100 mW/cm^2 laser irradiation, AlPcS2a-PICsomes exhibited remarkable increase in AlPcS2a fluorescence, and the rate further increased by increasing the laser power to 200 mW/cm^2. Note that free AlPcS2a showed slight decrease in the fluorescence after 20 min photoirradiation due to the photobleaching. The increased fluorescence intensities of AlPcS2a-PICsomes strongly suggest the photoinduced release of AlPcS2a from the PICsomes. We assume that singlet oxygen species (ROS) generated from AlPcS2a under irradiation might disturb the integrity of the PIC membranes of the PICsomes, leading to its increased permeability, although the reaction mechanism by ROS remains to be clarified.

Regarding the generation of ROS from AlPcS2a, we examined the photoinduced oxygen consumption rate of AlPcS2a-PICsomes and free AlPcS2a in PB (10 mM, pH 7.4) containing 10% fetal bovine serum (FBS) as singlet oxygen acceptor. The oxygen consumption efficiency method is considered as a reliable approach for measuring the production of reactive oxygen species (ROS) from AlPcS2a-loaded nanocarriers,[10] whereas the conventional method using fluorescent probes reactive to ROS might be sometimes inapplicable since relatively hydrophobic probes tend to concentrate in nanocontainers. As shown in Figure 1d, the oxygen consumption levels of AlPcS2a-PICsomes and free AlPcS2a reached ∼38 and ∼62%, respectively, within 12 min. Since the PIC membranes of the PICsomes exhibit semipermeable property,[2b] ROS seemed to be produced within the PICsomes and then rapidly distributed to the outside solution to react with FBS. Simultaneously, AlPcS2a released from the PICsomes, of which the process can be accelerated by the photochemical damage of the PIC membranes as aforementioned, may also partly contribute to the ROS production as well.

To evaluate the capability of the PICsomes to deliver AlPcS2a into cancer cells, we evaluated the cellular uptake and internalization pathways of AlPcS2a-PICsomes.[11] AlPcS2a-PICsomes and free AlPcS2a were incubated with A549 cells for 1, 4, 8, and 24 h, respectively, and the internalized amounts of AlPcS2a were measured by its fluorescence. As shown in Figure 2a, PICsomes exhibited time-dependent cellular uptake of AlPcS2a, and achieved 2-fold to 3-fold higher cellular uptake compared to free AlPcS2a. The AlPcS2a containing two sulfonate groups shows a negatively charged property in the extracellular space of tumor (pH between 6.5−6.8) and even in the more acidic lysosomes (pH 4.5−6.0) due to its very low pK_a values,[12] resulting in reduced cellular uptake. In contrast, AlPcS2a-PICsomes with neutral surface might show a promoted cellular uptake of AlPcS2a via endocytosis.

The internalization pathways of AlPcS2a-PICsomes in A549 cells were further studied using flow cytometry by applying various endocytosis inhibitors including chlorpromazine (inhibitor of clathrin-mediated endocytosis), filipin (inhibitor of caveolae-mediated endocytosis), nystatin (inhibitor of lipid raft-mediated uptake) and cytochalasin B (inhibitor of macropinocytosis).[11b,13] As shown in Figure 2b, the treatment with chlorpromazine at 10 μg/mL resulted in ∼53% decrease in the cellular uptake of AlPcS2a-PICsomes (Figure S2), suggesting that AlPcS2a-PICsomes might be mainly internalized via clathrin-mediated endocytic pathway, which generally plays a key role for the internalization of nanocontainers into cells.[13a] In addition, the treatment with cytochalasin B also led
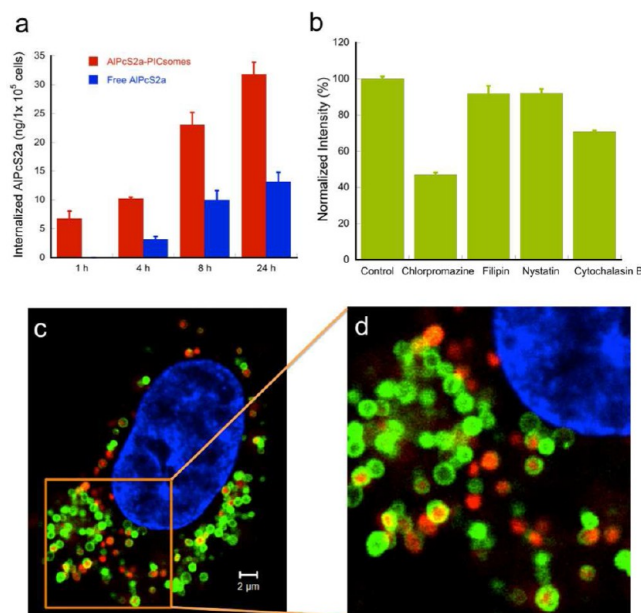

Figure 2. Cellular uptake and internalization pathways of AlPcS2a-PICsomes. (a) Amounts of internalized AlPcS2a by A549 cells (1 × 10^5) after 1, 4, 8, and 24 h of exposure to 1.0 μg/mL free AlPcS2a and AlPcS2a-PICsomes, respectively. (b) Normalized fluorescence intensity from AlPcS2a-PICsomes in A549 cells without (control) or with various inhibitors, including chlorpromazine (10 μg/mL), filipin (5 μg/mL), cytochalasin B (40 μg/mL), and nystatin (10 μg/mL), quantified by flow cytometry. (c) In vitro confocal imaging of subcellular distribution of AlPcS2a-PICsomes in A549 cells prestained by CellLight Lysosomes-GFP. Nuclei were stained with Hoechst 33342 (blue). (d) Enlarged view of selected area in (c).

to ∼30% decrease in cellular uptake, suggesting that macropinocytosis-mediated pathway might also partly contribute to cellular uptake of AlPcS2a-PICsomes. These pathways allow AlPcS2a-PICsomes to undergo the endo/lysosomal transport for intracellular delivery of AlPcS2a.

We next studied the intracellular distribution of AlPcS2a-PICsomes by confocal laser scanning microscopy (CLSM) utilizing the fluorescence of AlPcS2a (Ex: 633 nm; Em: 638−746 nm). The endo/lysosomal organelles in A549 cells were stained by LysoTracker Green DND-26. Moreover, the empty PICsomes were also traced by labeling the constituent polymer (PEG-P(Asp)-Cy3). As a result, both AlPcS2a-PICsomes and empty PICsomes were mainly distributed into endo/lysosomal compartments following internalization (Figures S3 and S4), and exhibited the colocalization levels of approximately 75% and 88% with LysoTracker Green DND-26, respectively. Since AlPcS2a with an amphiphilic property preferably distributes on endo/lysosomal membranes,[9b,14] we further performed a single cell observation using CLSM (LSM780) under 100×/1.46 oil-immersion lens to assess whether AlPcS2a-PICsomes were localized on endo/lysosomal membranes or inside endo/lysosomal compartments. In this study, we stained the lysosomal membranes by CellLight Lysosomes-GFP, which is a modified insect virus expressing a fusion construct of TagGFP and lysosomal associated membrane protein 1, Lamp1 protein. It enables a selective staining of lysosome membrane with >90% transduction efficiency in a wide range of mammalian cell lines.[15] By combination with a high-resolution fluorescent confocal microscopy, the lysosomes can be visualized as a spherical shape with single layer membrane (in green color)
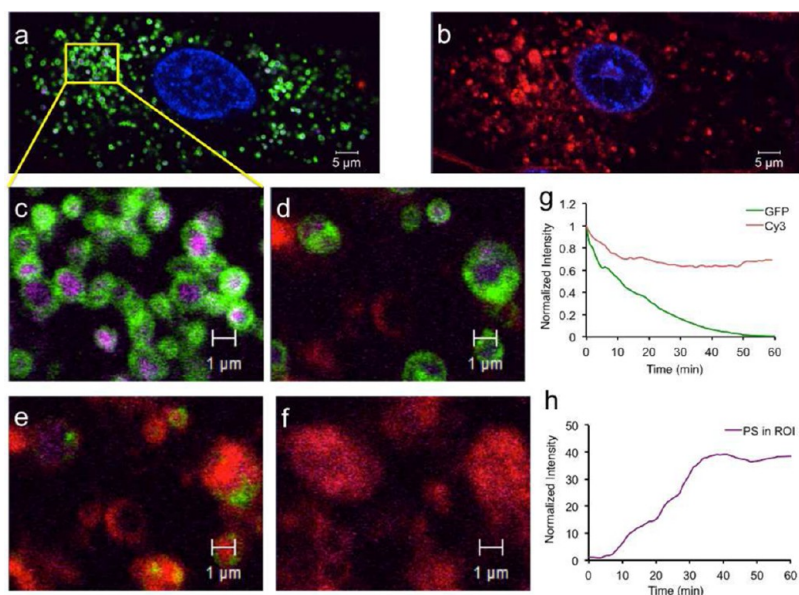
Figure 3. Change of AlPcS2a-PICsomes fluorescence in the lysosomes of single A549 cell under irradiation. In vitro confocal imaging of subcellular distribution of Cy3-labeled AlPcS2a-PICsomes (a) at the beginning and (b) after 60 min irradiation in single A549 cell prestained by CellLight Lysosomes-GFP (green fluorescence) (magenta: Cy3; red: AlPcS2a; blue: nucleus). A region of interest (ROI) in (a) was selected and imaged (c) before and after (d) 20 min, (e) 30 min, and (f) 60 min irradiation. The change of fluorescent signal intensities from (g) GFP-labeled lysosomes (GFP) and Cy3-labeled AlPcS2a-PICsomes (Cy3), and (h) AlPcS2a-PICsomes (AlPcS2a) during 60 min irradiation was quantified in the ROI.

(Figure 2c and d; green). After 4 h incubation with AlPcS2a-PICsomes, in A549 cells having their lysosomal membranes stained by CellLight Lysosomes-GFP (Figure 2c and d; green), the fluorescence of AlPcS2a within AlPcS2a-PICsomes (Figure 2c and d; red) was mainly distributed inside the lysosomal compartment (little colocalization of AlPcS2a and GFP-Lamp1). On the other hand, when A549 cells were incubated with free AlPcS2a, the fluorescence of AlPcS2a was mainly distributed on lysosomal membranes (appreciable colocalization of AlPcS2a and GFP-Lamp1), which was evident to undergo lysosomal disruption (PCI effect) and subsequent cytoplasm diffusion under light exposure, an intrinsic property of amphiphilic photosensitizer AlPcS2a (Figure S5).[13a,14b,c,16] These results suggested that AlPcS2a-PICsomes could be internalized and localized inside the lysosomal compartments with minimal release of AlPcS2a by circumventing its original lysosomal membrane localization. It is worth noting that, instead of generally describing lysosome localization using Lysotracker, we could discriminate between lysosomal membrane localization and lysosomal interior localization for the first time by the combination of a high-resolution fluorescent confocal microscopy and CellLight Lysosomes-GFP.

Next, in order to monitor the real-time behavior of AlPcS2a-PICsomes under irradiation in single cell, 30 min post incubation with Cy3-labeled AlPcS2a-PICsomes, a He−Ne laser (633 nm) was applied continuously over 60 min. As shown in Figure 3a and Supporting Information Video S1, Cy3 fluorescence (magenta) in Cy3 labeled AlPcS2a-PICsomes was surrounded by lysosomes with Lamp1-GFP (green) at the beginning of photoirradiation (30 min postincubation), indicating the localization of Cy3-labeled AlPcS2a-PICsomes inside the lysosomal compartments (Figure 3a and c). The changes in fluorescence intensities of Cy3-labeled AlPcS2a-PICsomes at a selected region of interest (ROI) in Figure 3a were calculated. The red fluorescence of AlPcS2a from the

PICsomes was significantly increased within the lysosomes after 7 min photoirradiation (Figure 3h), and gradually diffused from the lysosomal membranes to the cytoplasm (Figure 3d−f). Thus, the fluorescence intensity of AlPcS2a in ROI resulted in 38-fold increase after 60 min (Figure 3h). The quick increase in AlPcS2a (red) fluorescence observed under laser irradiation can be attributed to the aforementioned photoinduced release of AlPcS2a from the PICsomes. The subsequent diffusion of AlPcS2a can be explained by the PCI effect, where the lysosome membrane-located AlPcS2a induced photochemical disruption of lysosomal membranes via the generation of singlet oxygen, followed by the release of AlPcS2a into the cytosol.[11b,14b,c] Thus, AlPcS2a-PICsomes can exhibit photo-induced release of AlPcS2a even inside the cells, facilitating the cytoplasmic localization via the photochemical disruption of the lysosomal membranes (the PCI effect).

In terms of changes of GFP fluorescence (green, lysosomes) and Cy3 fluorescence (magenta, PICsomes), both were gradually decreased during photoirradiation (Figure 3c-3f and Figure 3g), suggesting the photochemical damage of the lysosomal membranes and the PIC membranes of the PICsomes by ROS produced from AlPcS2a, respectively. After 60 min photoirradiation, the GFP fluorescence (green) on the lysosomal membranes was largely disappeared (Figure 3b and 3f), and Cy3 fluorescence of PICsomes (magenta) diffused from the lysosomes to the cytosol (Video S3). The latter observation indicated the translocation of the PICsomes themselves from the lysosomal compartments to the cytoplasm by the PCI effect. Thus, the AlPcS2a-PICsomes might be useful for the photoinduced cytoplasmic delivery of cell membrane-impermeable drugs and macromolecular bioactive compounds, because the PICsomes can allow simultaneous incorporation of AlPcS2a and other molecules. Note that, the empty Cy3-labeled PICsomes (magenta) as the control were also internalized into the lysosomes with Lamp1-GFP (green), but was trapped in the lysosomal compartments all along during 60 min

photoirradiation as shown in Figure S6 and Video S2. It indicates that the empty PICsomes could neither escape lysosomal compartments in the absence of AlPcS2a, nor disrupt lysosomal membranes, as the lysosome was still intact (green).

To further confirm the intracellular behaviors of AlPcS2a-PICsomes, acridine orange (AO) was employed as an indicator of acid organelle integrity, which emits red fluorescence in lysosomes, and displays green fluorescence in the cytosol and nuclei.[6d,17] Figure 4b showed that acidic organelles in A549
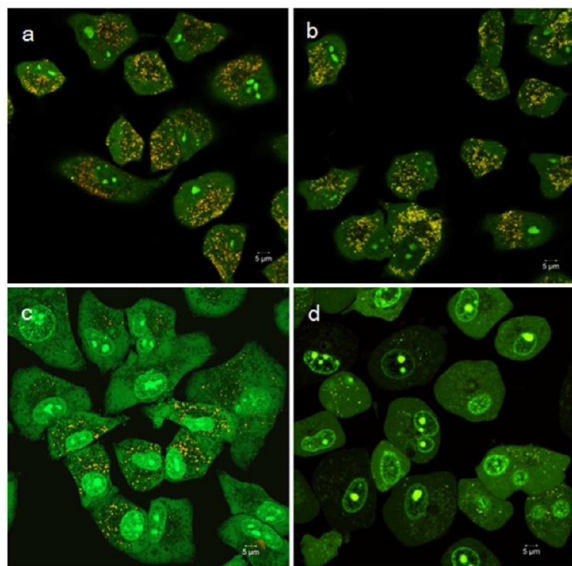

Figure 4. Observation of lysosomal disruption of A549 cells induced by AlPcS2a-PICsomes. The cells were treated with (a) PBS without irradiation, (b) light only, (c) AlPcS2a-PICsomes containing 0.05 μg/mL AlPcS2a, (d) AlPcS2a-PICsomes containing 0.2 μg/mL AlPcS2a, followed by 10 J/cm^2 laser application. The cells were further incubated with 6 μM AO for 15 min before CLSM analysis. (Ex: 488 nm; Em: 515−545 nm (green); 610−640 nm (red). AO as an intracellular indicator of acid organelle integrity emits red fluorescence in lysosomes, and displays green fluorescence in the cytosol and nuclei).

cells in the absence of AlPcS2a-PICsome displayed yellow fluorescence at a light dose of 10 J/cm^2 (33.3 mW/cm^2, 5 min with a 680 nm NIR laser), and exhibited no significant change compared to the untreated group (Figure 4a), indicating that the lysosomal compartments were maintained. However, under the same light exposure condition in the presence of PICsomes containing 0.05 μg/mL AlPcS2a, the yellow fluorescence from AO was remarkably decreased (Figure 4c). Furthermore, when the concentration of AlPcS2a in PICsomes reached 0.2 μg/mL, the yellow fluorescence from AO was strongly reduced (Figure 4d). These results indicate that the disruption of the lysosomal membranes is probably triggered by AlPcS2a, originating from the photoinduced release from the PICsomes as shown in Figure 1c. Photochemical disruption of the endo/lysosomal membranes is particularly important for those therapeutics targeting to cytoplasmic organelles after the endocytosis.

Next, the photocytotoxicity of AlPcS2a-PICsomes and free AlPcS2a was evaluated by MTT (3-(4,5-dimethylthiazol-2-yl)-2,5-diphenyltetrazolium bromide) assay[18] after 24 h incubation with A549 cells followed by 15, 30, and 45 min photoirradiation from a low power halogen lamp equipped with a filter passing light of 400−700 nm (fluence rate: 3.0 mW/cm^2; irradiation

time: 15, 30, and 45 min; fluence: 2.7, 5.4, and 8.1 J/cm^2). As shown in Figure 5, AlPcS2a-PICsomes exhibited 2-fold to 3-
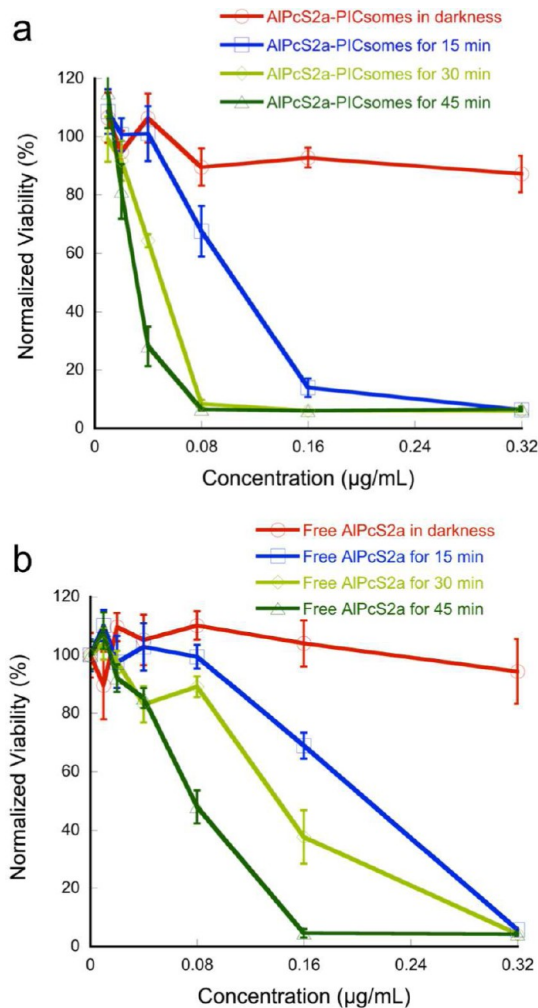

Figure 5. Photocytoxicity of (a) AlPcS2a-PICsomes and (b) free AlPcS2a against A549 cells, analyzed by MTT assay. The A549 cells were incubated with AlPcS2a-PICsomes and free AlPcS2a for 24 h, followed by 15, 30, and 45 min photoirradiation with a halogen lamp equipped with a bandpass filter (400−700 nm).

fold lower 50% cell growth-inhibitory concentration (IC$_{50}$) values than free AlPcS2a, suggesting superior phototoxicity of AlPcS2a-PICsomes over free AlPcS2a. The increased degree of cell death observed in AlPcS2a-PICsomes could be attributed to improved cellular uptake (Figure 2a), intracellular photo-induced AlPcS2a release from the PICsomes (Figure 1c), and subsequently maximized accessibility of AlPcS2a to cytoplasm (Figure 3c−f, 3h).

To clarify the mechanism of cell death induced by AlPcS2a-PICsomes under light irradiation, we analyzed both early and later apoptosis using annexin V-FITC/PI assay (Figure S7). It was found that minimal apoptosis was observed in the cells exposed to 0.32 μg/mL AlPcS2a-PICsomes in the dark (2.9% for early apoptosis; 6.6% for later apoptosis; 0.8% for necrosis) (Figure S7c) or those with light exposure (3.0 mW/cm^2, 15 min) but without preincubation with AlPcS2a-PICsomes (1.7% for early apoptosis; 5.4% for later apoptosis; 0.3% for necrosis) (Figure S7b), compared to an untreated control (2.0% for early apoptosis; 4.5% for later apoptosis; 0.8% for necrosis) (Figure

S7a). However, under the same light exposure, cells in the presence of 0.32 μg/mL AlPcS2a-PICsomes induced significantly apoptosis (22.8% for early apoptosis; 30.9% for later apoptosis; 2.7% for necrosis) (Figure S7d). Regarding the mechanisms of cell death, it is reported that the target of PDT is not limited to endo/lysosomes. Other cellular organelles, such as mitochondria, nucleus, endoplasmic reticulum, and Golgi complex, may also partly contribute to cell death.[19] The mitochondria, for example, has been shown to be a critical target in PDT because it is the main organelle involved in apoptosis.[19b] Additionally, the disruption of lysosomal membranes possibly leads to the release of lysosomal enzymes such as hydrolases and proteases into cytosol. The hydrolases and proteases can degrade antiapoptotic Bcl-2 proteins and cleave Bid (a Bcl-2 homologue), which subsequently results in the release of cytochrome *c* from mitochondria, amplifying apoptotic signals and eventually initiating the apoptotic pathway.[17,19c,20] Moreover, the destabilization of lysosomes can further prevent cancer cells from autophagy based rescue, which is a protective role in apoptosis process and thereby contribute to apoptosis.[14a,20a] Although the mechanisms of cell death remain to be clarified, the disruption of lysosomes may be highly advantageous for maximizing the photocytotoxicity.

CONCLUSION

In conclusion, we demonstrated photoinduced release of AlPcS2a from the PICsomes. The combination of a high-resolution fluorescent confocal microscopy and lysosome membrane-specific staining using CellLight Lysosomes-GFP revealed that photoinduced release of AlPcS2a from the PICsomes occurred in the lysosomal compartments of living cells, facilitating the translocation of AlPcS2a and PICsomes themselves to the cytoplasm based on the PCI effect. This process was more efficient as compared to the conventional PCI using free AlPcS2a, as the AlPcS2a-PICsomes showed 2-fold to 3-fold stronger photocytotoxicity compared with free AlPcS2a alone. These results suggest the potential utility of the AlPcS2a-PICsomes for PDT and PCI. It is intriguing that the PICsomes can encapsulate various compounds just by a simple vortex mixing, allowing photoinduced cytoplasmic delivery of functional macromolecules, such as membrane-impermeable nucleic acids, radiotherapeutic agents, or anticancer compounds.

ASSOCIATED CONTENT

S Supporting Information

Experimental procedures, fluorescent spectrum, inhibitors study, intracellular distribution, and apoptosis study. This material is available free of charge via the Internet at http://pubs.acs.org.

AUTHOR INFORMATION

Corresponding Authors
kishimura@mail.cstm.kyushu-u.ac.jp
nishiyama@res.titech.ac.jp
kataoka@bmw.t.u-tokyo.ac.jp

Author Contributions
○H.C. and L.X. contributed equally.

Notes
The authors declare no competing financial interest.

REFERENCES

(1) (a) Xiong, X. B.; Uludag, H.; Lavasanifar, A. *Biomaterials* **2009**, *30*, 242−253. (b) Lee, H. J.; Bae, Y. *Biomacromolecules* **2011**, *12*, 2686−2696. (c) Bae, Y.; Kataoka, K. *Adv. Drug Delivery Rev.* **2009**, *61*, 768−784. (d) Peer, D.; Karp, J. M.; Hong, S.; Farokhzad, O. C.; Margalit, R.; Langer, R. *Nat. Nanotechnol.* **2007**, *2*, 751−760.

(2) (a) Koide, A.; Kishimura, A.; Osada, K.; Jang, W. D.; Yamasaki, Y.; Kataoka, K. *J. Am. Chem. Soc.* **2006**, *128*, 5988−5989. (b) Anraku, Y.; Kishimura, A.; Oba, M.; Yamasaki, Y.; Kataoka, K. *J. Am. Chem. Soc.* **2010**, *132*, 1631−1636. (c) Anraku, Y.; Kishimura, A.; Kobayashi, A.; Oba, M.; Kataoka, K. *Chem. Commun.* **2011**, *47*, 6054−6056. (d) Kishimura, A.; Koide, A.; Osada, K.; Yamasaki, Y.; Kataoka, K. *Angew Chem., Int. Ed.* **2007**, *46*, 6085−6088.

(3) (a) Yano, S.; Hirohara, S.; Obata, M.; Hagiya, Y.; Ogura, S.; Ikeda, A.; Kataoka, H.; Tanak, M.; Joh, T. *J. Photochem. Photobiol., C* **2011**, *12*, 46−67. (b) Chatterjee, D. K.; Fong, L. S.; Zhang, Y. *Adv. Drug Delivery Rev.* **2008**, *60*, 1627−1637.

(4) (a) Norum, O. J.; Selbo, P. K.; Weyergang, A.; Giercksky, K. E.; Berg, K. *J. Photochem. Photobiol. B* **2009**, *96*, 83−92. (b) Selbo, P. K.; Weyergang, A.; Hogset, A.; Norum, O. J.; Berstad, M. B.; Vikdal, M.; Berg, K. *J. Controlled Release* **2010**, *148*, 2−12. (c) Hogset, A.; Prasmickaite, L.; Selbo, P. K.; Hellum, M.; Engesaeter, B. O.; Bonsted, A.; Berg, K. *Adv. Drug Delivery Rev.* **2004**, *56*, 95−115.

(5) Matsumura, Y.; Maeda, H. *Cancer Res.* **1986**, *46*, 6387−6392.

(6) (a) Nishiyama, N.; Morimoto, Y.; Jang, W. D.; Kataoka, K. *Adv. Drug Delivery Rev.* **2009**, *61*, 327−338. (b) Paszko, E.; Ehrhardt, C.; Senge, M. O.; Kelleher, D. P.; Reynolds, J. V. *Photodiagn. Photodyn. Ther.* **2011**, *8*, 14−29. (c) Nishiyama, N.; Nakagishi, Y.; Morimoto, Y.; Lai, P. S.; Miyazaki, K.; Urano, K.; Horie, S.; Kumagai, M.; Fukushima, S.; Cheng, Y.; Jang, W. D.; Kikuchi, M.; Kataoka, K. *J. Controlled Release* **2009**, *133*, 245−251. (d) Lu, H. L.; Syu, W. J.; Nishiyama, N.; Kataoka, K.; Lai, P. S. *J. Controlled Release* **2011**, *155*, 458−464. (e) Li, W. T. *Curr. Drug Metab.* **2009**, *10*, 851−860. (f) Ding, H.; Sumer, B. D.; Kessinger, C. W.; Dong, Y.; Huang, G.; Boothman, D. A.; Gao, J. *J. Controlled Release* **2011**, *151*, 271−277. (g) Lee, S. J.; Koo, H.; Jeong, H.; Huh, M. S.; Choi, Y.; Jeong, S. Y.; Byun, Y.; Choi, K.; Kim, K.; Kwon, I. C. *J. Controlled Release* **2011**, *152*, 21−29. (h) Yoon, H. Y.; Koo, H.; Choi, K. Y.; Lee, S. J.; Kim, K.; Kwon, I. C.; Leary, J. F.; Park, K.; Yuk, S. H.; Park, J. H.; Choi, K. *Biomaterials* **2012**, *33*, 3980−3989. (i) Jeong, H.; Huh, M.; Lee, S. J.; Koo, H.; Kwon, I. C.; Jeong, S. Y.; Kim, K. *Theranostics* **2011**, *1*, 230−239. (j) Jin, C. S.; Zheng, G. *Lasers Surg. Med.* **2011**, *43*, 734−748. (k) Gaware, V. S.; Hakerud, M.; Leosson, K.; Jonsdottir, S.; Hogset, A.; Berg, K.; Masson, M. *J. Med. Chem.* **2013**, *56*, 807−819.

(7) (a) Derycke, A. S.; de Witte, P. A. *Adv. Drug Delivery Rev.* **2004**, *56*, 17−30. (b) Brinkhuis, R. P.; Rutjes, F. P. J. T.; van Hest, J. C. M. *Polym. Chem.* **2011**, *2*, 1449−1462. (c) Tanner, P.; Baumann, P.; Enea, R.; Onaca, O.; Palivan, C.; Meier, W. *Acc. Chem. Res.* **2011**, *44*, 1039−1049.

(8) Brus, C.; Petersen, H.; Aigner, A.; Czubayko, F.; Kissel, T. *Bioconjugate Chem.* **2004**, *15*, 677−684.

(9) (a) Phillips, D.; Dhami, S.; Ostler, R.; Petrasek, Z. *Prog. React. Kinet. Mech.* **2003**, *28*, 299−420. (b) Wang, J. T. W.; Berg, K.; Hogset, A.; Bown, S. G.; MacRobert, A. J. *Photochem. Photobiol. Sci.* **2013**, *12*, 519−526.

(10) (a) Jang, W. D.; Nishiyama, N.; Zhang, G. D.; Harada, A.; Jiang, D. L.; Kawauchi, S.; Morimoto, Y.; Kikuchi, M.; Koyama, H.; Aida, T.; Kataoka, K. *Angew Chem., Int. Ed.* **2005**, *44*, 419−423. (b) Baier, J.; Maisch, T.; Regensburger, J.; Loibl, M.; Vasold, R.; Baumler, W. *J. Biomed. Opt.* **2007**, *12*, 064008.

(11) (a) Herlambang, S.; Kumagai, M.; Nomoto, T.; Horie, S.; Fukushima, S.; Oba, M.; Miyazaki, K.; Morimoto, Y.; Nishiyama, N.; Kataoka, K. *J. Controlled Release* **2011**, *155*, 449−457. (b) Iversen, T. G.; Skotland, T.; Sandvig, K. *Nano Today* **2011**, *6*, 176−185.

(12) Berg, K.; Nordstrand, S.; Selbo, P. K.; Diem, T. T. T.; Angell-Petersen, E.; Hogset, A. *Photoch. Photobio. Sci.* **2011**, *10*, 1637−1651.

(13) (a) Huang, J. G.; Leshuk, T.; Gu, F. X. *Nano Today* **2011**, *6*, 478−492. (b) McLendon, P. M.; Fichter, K. M.; Reineke, T. M. *Mol. Pharmaceutics* **2010**, *7*, 738−750. (c) Gratton, S. E. A.; Ropp, P. A.; Pohlhaus, P. D.; Luft, J. C.; Madden, V. J.; Napier, M. E.; DeSimone, J. M. *Proc. Natl. Acad. Sci. U.S.A.* **2008**, *105*, 11613−11618. (d) Santos, T. D.; Varela, J.; Lynch, I.; Salvati, A.; Dawson, K. A. *PLoS One* **2011**, *6*, e24438.

(14) (a) Hung, Y. H.; Chen, L. M.; Yang, J. Y.; Yang, W. Y. *Nat. Commun.* **2013**, *4*, 2111. (b) Selbo, P. K.; Sivam, G.; Fodstad, O.; Sandvig, K.; Berg, K. *Int. J. Cancer* **2001**, *92*, 761−766. (c) Selbo, P. K.; Sandvig, K.; Kirveliene, V.; Berg, K. *Biochem. Biophys. Acta* **2000**, *1475*, 307−313.

(15) (a) Kost, T. A.; Condreay, J. P.; Jarvis, D. L. *Nat. Biotechnol.* **2005**, *23*, 567−575. (b) Falcón-Pérez, J. M.; Nazarian, R.; Sabatti, C.; Dell'Angelica, E. C. *J. Cell Sci.* **2005**, *118*, 5243−5255.

(16) Prasmickaite, L.; Hogset, A.; Berg, K. *Photochem. Photobiol.* **2001**, *73*, 388−395.

(17) Boya, P.; Kroemer, G. *Oncogene* **2008**, *27*, 6434−6451.

(18) (a) Mosmann, T. *J. Immunol. Methods* **1983**, *65*, 55−63. (b) Carmichael, J.; Degraff, W. G.; Gazdar, A. F.; Minna, J. D.; Mitchell, J. B. *Cancer Res.* **1987**, *47*, 936−942.

(19) (a) Teiten, M. H.; Bezdetnaya, L.; Morliere, P.; Santus, R.; Guillemin, F. *Br. J. Cancer* **2003**, *88*, 146−152. (b) Hilf, R. *J. Bioenerg. Biomembr.* **2007**, *39*, 85−89. (c) Repnik, U.; Cesen, M. H.; Turk, B. *Cold Spring Harbor Perspect. Biol.* **2013**, *5*, a008755. (d) Nishiyama, N.; Iriyama, A.; Jang, W. D.; Miyata, K.; Itaka, K.; Inoue, Y.; Takahashi, H.; Yanagi, Y.; Tamaki, Y.; Koyama, H.; Kataoka, K. *Nat. Mater.* **2005**, *4*, 934−941.

(20) (a) Repnik, U.; Turk, B. *Mitochondrion* **2010**, *10*, 662−669. (b) Repnik, U.; Stoka, V.; Turk, V.; Turk, B. *Biochim. Biophys. Acta* **2012**, *1824*, 22−33. (c) Oleinick, N. L.; Morris, R. L.; Belichenko, I. *Photochem. Photobiol. Sci.* **2002**, *1*, 1−21.